Scientific Research Publishing

Applied Mathematics, 2024, 15, 568-583
https://www.scirp.org/journal/am
ISSN Online: 2152-7393
ISSN Print: 2152-7385

Heat and Mass Transfer on Non-Newtonian Peristaltic Flow in a Channel in Presence of Magnetic Field: Analytical and Numerical Analysis

Md. Maruf Hasan[1*], Md. Enamul Karim[1], Md. Abdus Samad[2]

[1]Department of Mathematics, Comilla University, Comilla, Bangladesh
[2]Department of Applied Mathematics, University of Dhaka, Dhaka, Bangladesh
Email: *marufek@yahoo.com

How to cite this paper: Hasan, Md.M., Karim, Md.E. and Samad, Md.A. (2024) Heat and Mass Transfer on Non-Newtonian Peristaltic Flow in a Channel in Presence of Magnetic Field: Analytical and Numerical Analysis. *Applied Mathematics*, **15**, 568-583.
https://doi.org/10.4236/am.2024.158034

Received: July 28, 2024
Accepted: August 24, 2024
Published: August 27, 2024

Abstract

A study has been arranged to investigate the flow of non-Newtonian fluid in a vertical asymmetrical channel using peristalsis. The porous medium allows the electrically conductive fluid to flow in the channel, while a uniform magnetic field is applied perpendicular to the flow direction. The analysis takes into account the combined influence of heat and mass transfer, including the effects of Soret and Dufour. The flow's non-Newtonian behavior is characterized using a Casson rheological model. The fluid flow equations are examined within a wave frame of reference that has a wave velocity. The analytic solution is examined using long wavelengths and a small Reynolds number assumption. The stream function, temperature, concentration and heat transfer coefficient expressions are derived. The bvp4c function from MATLAB has been used to numerically solve the transformed equations. The flow characteristics have been analyzed using graphs to demonstrate the impacts of different parameters.

Keywords

Stream Function, Mass Transfer, Vertical Channel, Casson Fluid

1. Introduction

The study of peristaltic flows has been an important topic over the last few decades. It is one of the major mechanisms for fluid transport in many biological systems and industrial pumping. This property is naturally associated with a progressive wave of area expansion and contraction along the length of a flu-

id-filled channel, mixing and transporting the fluid in the direction of the wave propagation. Peristaltic mechanism in the channel has a wide range of physiological applications, for example, urine transports from the kidney to the bladder, swallowing food material through the esophagus, semen movement in the vas deferens of the male reproductive tract and blood circulation in small blood vessels. The initial work on peristaltic mechanism in a viscous fluid was conducted by Latham [1] and after that, we found many studies [2]-[9].

The study of heat transfer analysis is a significant area in connection with peristaltic motion. Such flows with heat transfer have many applications in biomedical sciences and industry such as the analysis of tissues, blood oxygenation, dialysis, crude oil refinement and food processing [10]. Again mass transfer occurs in many industrial processes such as reverse osmosis, filtration process, distillation process etc. When heat and mass transfer occur at the same time, the fluid behavior becomes more complicated due to the fact that energy flux is produced not only by temperature differences but also by concentration variances. Dufour effects, also known as diffusion thermo effects, arise from the energy flux caused by mass concentration gradients. These effects are the reverse of Soret effects, which are produced by temperature gradients. So we can't neglect such effects when density difference exists in the flow regime.

The majority of physiological and industrial fluids are recognized to have non-Newtonian properties. One constitutive equation is insufficient to explain all non-Newtonian fluids. Consequently, several non-Newtonian fluid models have been put forth. Casson fluid is among those non-Newtonian fluids. Casson [11] was the one who initially presented this Casson model. Casson fluid is characterized as a shear-thinning liquid, with its viscosity decreasing as the shear rate increases. It is assumed to have extremely high viscosity at zero shear rate and it exhibits a yield stress below which no flow occurs, as well as zero viscosity at extremely high shear rates. This type of fluid demonstrates behavior similar to elastic solids and features a yield shear stress in its constitutive equation. The application of Casson fluids is observed in the development of models for blood oxygenator and haemodialysis processes. According to Blair and Spanner [12], blood from humans can be described using Casson's model. The available research indicates that the peristaltic motion of Casson fluid in a channel subjected to a magnetic field is not properly considered. The goal of the study is to close this gap.

2. Mathematical Modeling

Consider the impacts of heat and mass transfer in the flow of a non-Newtonian Casson fluid that is incompressible and electrically conducting in a two-dimensional asymmetric vertical channel. The Y-axis is normal to the channel, while the X-axis is measured along its length in this instance. Constant concentrations C_0 and C_1, as well as constant temperatures T_0 and T_1, are maintained for the channel walls H_1 and H_2. The Y direction is subjected to a constant magnetic field B_0.

In many flow problems, the electrostatic force can be considered insignificant compared to the electromagnetic force. The dynamics of an electrically conducting fluid depend significantly on the interaction between the magnetic field and the flow. A substantial impact on the flow field occurs when the electromagnetic force is perpendicular to both the magnetic field and the current density. Hence, the flow field is significantly influenced by the direction of the magnetic field. (Figure 1)

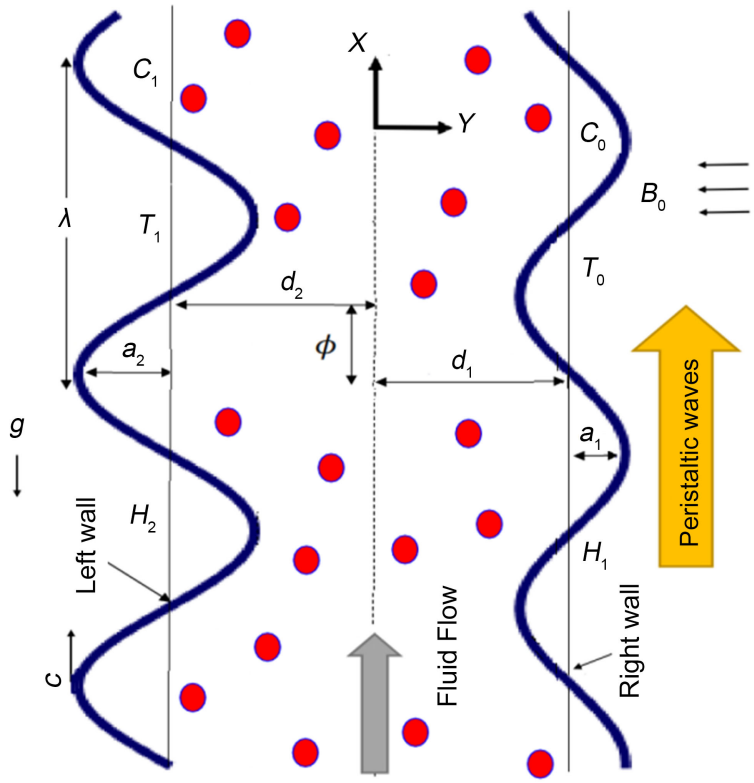

Figure 1. Geometry of the model.

$$\left.\begin{aligned} Y = H_1 &= d_1 + a_1 \cos\left\{\frac{2\pi}{\lambda}(X - ct)\right\} \\ Y = H_2 &= -d_2 - a_2 \cos\left\{\frac{2\pi}{\lambda}(X - ct) + \phi\right\} \end{aligned}\right\} \tag{1}$$

While $d_1 + d_2$ representing the channel width, a_1, a_2 indicate the wave amplitudes. The variables λ, t, c and ϕ represent the wavelength, time, propagation velocity, and phase difference, respectively.

The constitutive equation for Casson fluid [13] [14] is as

$$\tau_{ij} = 2\left(\mu_b + \frac{P_y}{\sqrt{2\pi}}\right)e_{ij} \tag{2}$$

The governing equations for this model are

$$\frac{\partial U}{\partial X} + \frac{\partial V}{\partial Y} = 0 \tag{3}$$

$$\begin{aligned}&\frac{\partial U}{\partial t}+U\frac{\partial U}{\partial X}+V\frac{\partial U}{\partial Y}\\&=-\frac{1}{\rho}\frac{\partial P}{\partial X}+\nu\left(1+\frac{1}{\beta}\right)\left(\frac{\partial^2 U}{\partial X^2}+\frac{\partial^2 U}{\partial Y^2}\right)-\frac{\sigma B_0^2}{\rho}U-\nu\left(1+\frac{1}{\beta}\right)\frac{U}{K'}\\&\quad+g\beta_T\left(T-T_0\right)+g\beta_c\left(C-C_0\right)\end{aligned}\tag{4}$$

$$\frac{\partial V}{\partial t}+U\frac{\partial V}{\partial X}+V\frac{\partial V}{\partial Y}=-\frac{1}{\rho}\frac{\partial P}{\partial Y}+\nu\left(1+\frac{1}{\beta}\right)\left(\frac{\partial^2 V}{\partial X^2}+\frac{\partial^2 V}{\partial Y^2}\right)-\nu\left(1+\frac{1}{\beta}\right)\frac{V}{K'}\tag{5}$$

$$\begin{aligned}&\frac{\partial T}{\partial t}+U\frac{\partial T}{\partial X}+V\frac{\partial T}{\partial Y}\\&=\frac{k}{\rho C_p}\left(\frac{\partial^2 T}{\partial X^2}+\frac{\partial^2 T}{\partial Y^2}\right)+\frac{Q}{\rho C_p}-\frac{1}{\rho C_p}\left(\frac{\partial q_r}{\partial X}+\frac{\partial q_r}{\partial Y}\right)+\frac{DK_T}{c_s}\left(\frac{\partial^2 C}{\partial X^2}+\frac{\partial^2 C}{\partial Y^2}\right)\end{aligned}\tag{6}$$

$$\frac{\partial C}{\partial t}+U\frac{\partial C}{\partial X}+V\frac{\partial C}{\partial Y}=D\left(\frac{\partial^2 C}{\partial X^2}+\frac{\partial^2 C}{\partial Y^2}\right)+\frac{DK_T}{T_m}\left(\frac{\partial^2 T}{\partial X^2}+\frac{\partial^2 T}{\partial Y^2}\right)\tag{7}$$

The related boundary conditions are

$$\left.\begin{aligned}&U=0,\ T=T_0,\ C=C_0 \quad \text{at } Y=H_1\\&U=0,\ T=T_1,\ C=C_1 \quad \text{at } Y=H_2\end{aligned}\right\}\tag{8}$$

The radiative heat flux q_r is defined by

$$q_r=-\frac{16\sigma^* T_0^3}{3k^*}\frac{\partial T}{\partial Y}\tag{9}$$

where σ^* is the Stefan-Boltzmann constant and k^* is the absorption coefficient.

The relationship between the coordinates in the fixed frame and wave frame can be expressed as follows.

$$\left.\begin{aligned}&x=X-ct,\ y=Y,\ u=U-c,\ v=V,\ p\left(x,y\right)=P\left(X,Y,t\right)\\&\bar{T}\left(x,y\right)=T\left(X,Y,t\right),\ \bar{C}\left(x,y\right)=C\left(X,Y,t\right),\end{aligned}\right\}\tag{10}$$

The following dimensionless quantities are now being introduced.

$$\left.\begin{aligned}&x'=\frac{x}{\lambda},\ y'=\frac{y}{d_1},\ u'=\frac{u}{c},\ v'=\frac{v}{c\delta},\ t'=\frac{ct}{\lambda},\ p'=\frac{pd_1^2}{\lambda c\mu_b},\ \delta=\frac{d_1}{\lambda}\\&h_1=\frac{H_1}{d_1},\ h_2=\frac{H_2}{d_1},\ d=\frac{d_2}{d_1},\ a=\frac{a_1}{d_1},\ b=\frac{a_2}{d_1},\ \theta=\frac{\bar{T}-\bar{T}_0}{\bar{T}_1-\bar{T}_0},\ \varphi=\frac{\bar{C}-\bar{C}_0}{\bar{C}_1-\bar{C}_0}\end{aligned}\right\}\tag{11}$$

When considering physiological processes, it is important to acknowledge the significance of long wavelengths as they play a critical role in the propagation of waves in vessels. On the other hand, a low Reynolds number means viscous force is predominant and the effect of viscosity will be felt in the whole flow field. Taking into account long wavelengths and small amplitudes is essential to prevent the bending rigidity of vessel walls. Long wavelengths form the basis for technologies such as amplitude modulation, frequency modulation radios, lasers utilized in cosmetic procedures and radar systems for airplanes. The equations governing (3)-(7) when assuming long wavelengths and low Reynolds numbers, expressed in terms of the stream function ψ without the dash symbols, transform

to the following.

$$\frac{\partial p}{\partial x}=\left(1+\frac{1}{\beta}\right)\frac{\partial^3\psi}{\partial y^3}-M^2\left(\frac{\partial\psi}{\partial y}+1\right)-\left(1+\frac{1}{\beta}\right)\frac{1}{K}\left(\frac{\partial\psi}{\partial y}+1\right)+Gr\theta+Gc\varphi \tag{12}$$

$$\frac{\partial p}{\partial y}=0 \tag{13}$$

$$\left(1+Rd\right)\theta''+Q_0+PrDu\varphi''=0 \tag{14}$$

$$\varphi''+ScSr\theta''=0 \tag{15}$$

The dimensionless boundary conditions become

$$\left.\begin{aligned}\psi=\frac{F}{2},\ \frac{\partial\psi}{\partial y}=-1,\ \theta=0,\ \varphi=0 \quad \text{at } y=h_1\\ \psi=-\frac{F}{2},\ \frac{\partial\psi}{\partial y}=-1,\ \theta=1,\ \varphi=1 \quad \text{at } y=h_2\end{aligned}\right\} \tag{16}$$

where $M=\sqrt{\frac{\sigma}{\mu_b}}B_0d_1$ is the magnetic field parameter, $K=\frac{K'}{d_1^2}$ is the permeability parameter, F is the volume flow rate in the wave frame, $\beta=\frac{\mu_b\sqrt{2\pi}}{P_y}$ is the Casson fluid parameter, $Gr=\frac{g\beta_T\left(\bar{T}_1-\bar{T}_0\right)d_1^2}{c\nu}$ is the temperature Grashof number, $Gc=\frac{g\beta_c\left(\bar{C}_1-\bar{C}_0\right)d_1^2}{c\nu}$ is the concentration Grashof number, $Pr=\frac{\rho\nu C_p}{k}$ is the Prandtl number, $Rd=\frac{16T_0^3\sigma^*}{3kk^*}$ is the radiation parameter, $Q_0=\frac{Qd_1^2}{k\left(\bar{T}_1-\bar{T}_0\right)}$ is the heat generation parameter, $Du=\frac{DK_T\left(\bar{C}_1-\bar{C}_0\right)}{\mu_bC_pc_s\left(\bar{T}_1-\bar{T}_0\right)}$ is the Dufour number, $Sc=\frac{\nu}{D}$ is the Schmidt number and $Sr=\frac{DK_T\left(\bar{T}_1-\bar{T}_0\right)}{T_m\nu\left(\bar{C}_1-\bar{C}_0\right)}$ is the Soret number.

3. Analytic Solution

Equation (13) gives that $p\neq p(y)$. Eliminating the pressure terms from (12) we get

$$\frac{\partial^4\psi}{\partial y^4}-\alpha^2\frac{\partial^2\psi}{\partial y^2}+\frac{\beta}{1+\beta}\left(Gr\theta'+Gc\varphi'\right)=0 \tag{17}$$

Solving equations (14) and (15) with the boundary conditions (16), the temperature and concentration are obtained as

$$\theta=-\frac{Ay^2}{2}+A_1y+A_2 \tag{18}$$

$$\varphi=ScSrA\frac{y^2}{2}+B_1y+B_2 \tag{19}$$

Using the above solutions and boundary conditions (16) in (17), we get the stream function as

$$\psi = C_1 + C_2 y + C_3 \mathrm{e}^{\alpha y} + C_4 \mathrm{e}^{-\alpha y} + C_5 y^2 + C_6 y^3 \tag{20}$$

The dimensionless mean flow rate Q' is given by

$$Q' = F + 1 + d \tag{21}$$

in which

$$F = \int_{h_2}^{h_1} u \mathrm{d}y \tag{22}$$

Notice that h_1 and h_2 symbolize the dimensionless versions of the peristaltic walls.

$$\left.\begin{aligned} h_1 &= 1 + a\cos 2\pi x \\ h_2 &= -d - b\cos\left(2\pi x + \phi\right) \end{aligned}\right\} \tag{23}$$

Again the heat transfer coefficient at the right wall $\left(y = h_1\right)$ is once again

$$Z_1 = h_{1x}\theta' = 2\pi a\left(Ay - A_1\right)\sin\left(2\pi x\right) \tag{24}$$

4. Numerical Solution

The built-in bvp4c function in MATLAB has also been utilized to solve the equations. The following parameter values have been utilized in order to obtain a numerical result: $a = 0.4$, $b = 0.5$, $d = 1.3$, $F = 0.2$, $x = 0.1$, $M = 1$, $K = 0.5$, $\beta = 1$, $Gr = 0.5$, $Q_0 = 0.5$, $Rr = 1$, $\phi = \pi/4$, $Gc = 0.3$, $Du = 0.3$, $Sc = 0.5$, $Sr = 0.3$, unless otherwise specified.

5. Results and Discussions

Figure 2 shows the dependence of the magnetic field parameter M on the velocity component u. This illustrates the parabolic character of the velocity profile. It is evident that as M is raised, u falls off close to the channel's center. An electrical conduction flow subjected to an applied magnetic field produces a resistive force known as the Lorenz force. The fluid's mobility is prone to being slowed down by this force. The impact on the velocity field is so lessening. So we say that the magnetic field has the ability to influence the increase in fluid viscosity. The speed of the fluid flow is also decreased, allowing for control of fluid velocity due to this characteristic. As the permeability parameter K increases, velocity also increases, as seen in Figure 3. Figure 4 shows how the Casson fluid parameter β affects velocity. The parameter β is defined as the ratio of plastic dynamic viscosity to yield stress. Therefore, an increase β indicates a decrease in yield stress (as larger β values indicate the fluid behaves more like a Newtonian fluid, causing it to deviate from Casson flow), leading to an acceleration of the fluid flow. Figure 5 shows the effect of radiation parameter Rd on velocity. It was observed that toward the center of the channel with the largest Rd, the velocity profile's magnitude increases.

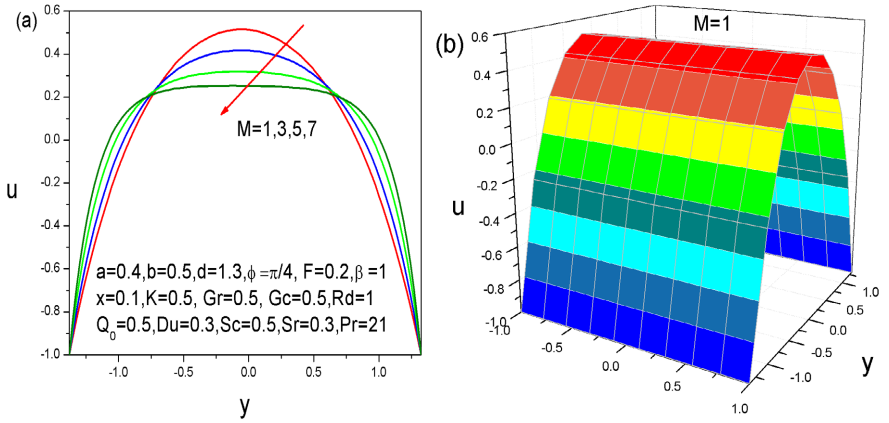

Figure 2. Velocity profiles for different M (a) 2D and (b) 3D.

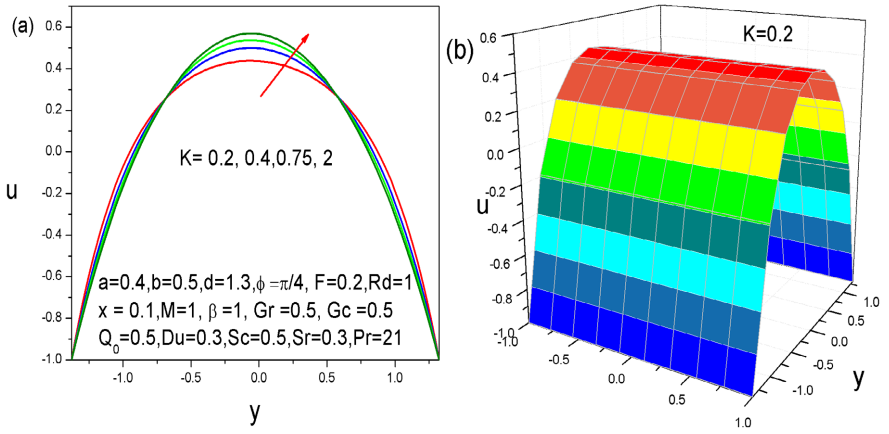

Figure 3. Velocity profiles for different K (a) 2D and (b) 3D.

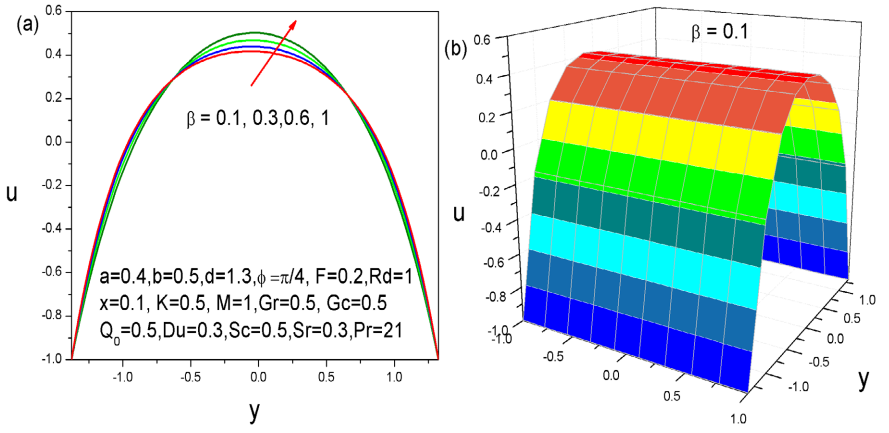

Figure 4. Velocity profiles for different β (a) 2D and (b) 3D.

Figure 6 shows the impact of the Dufour number Du. The Dufour number represents the ratio of concentration gradients to thermal energy flux in the flow. The temperature rises due to an increase in Dufour number Du. Figure 7 shows how the radiation parameter Rd affects the temperature field. The temperature inside the channel drops as a result of the higher Rd values, which indicate a higher surface heat flux.

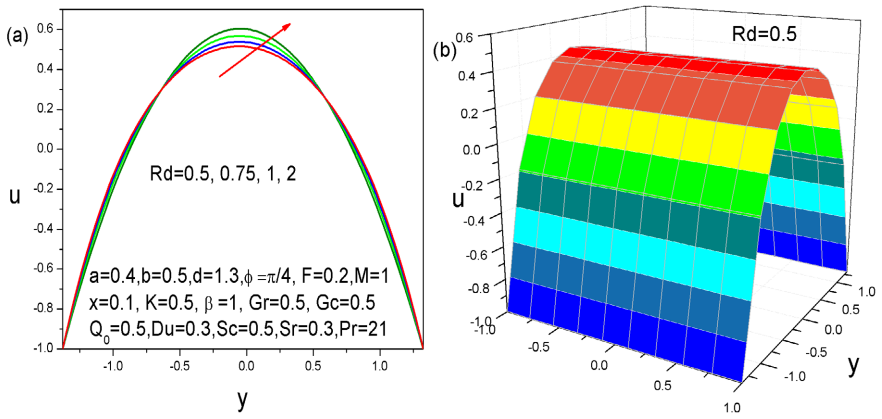

Figure 5. Velocity profiles for different *Rd* (a) 2D and (b) 3D.

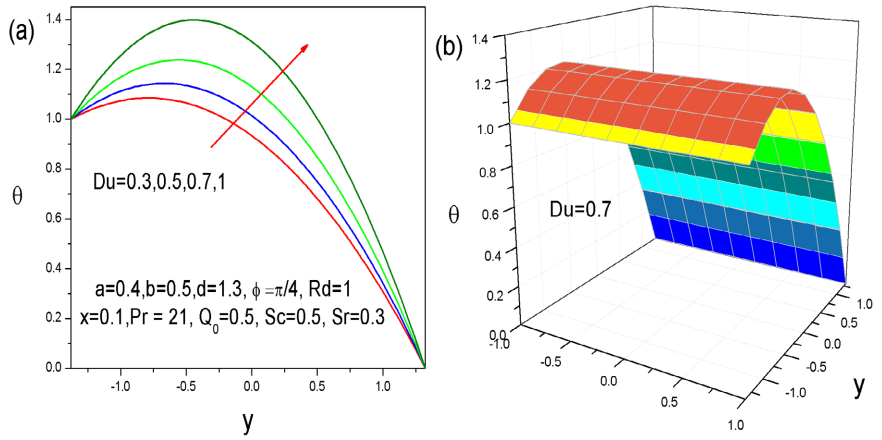

Figure 6. Temperature profiles for different *Du* (a) 2D and (b) 3D.

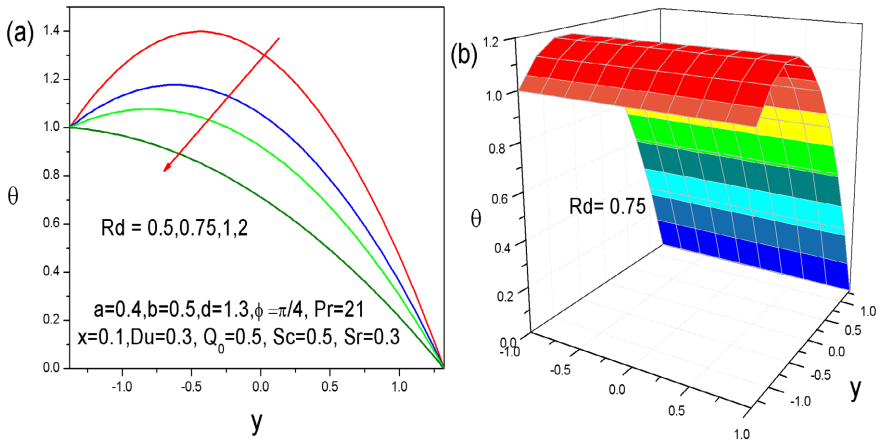

Figure 7. Temperature profiles for different *Rd* (a) 2D and (b) 3D.

Figure 8 shows the concentration profiles for various Schmidt number *Sc* values. The ratio of mass diffusivity to momentum diffusivity is denoted by *Sc*. In this case, when *Sc* increases the profile falls. **Figure 9** shows the impact of Soret number *Sr* on concentration profiles. The Soret number represents the ratio of temperature difference to concentration. The concentration profile declines as *Sr* increases.

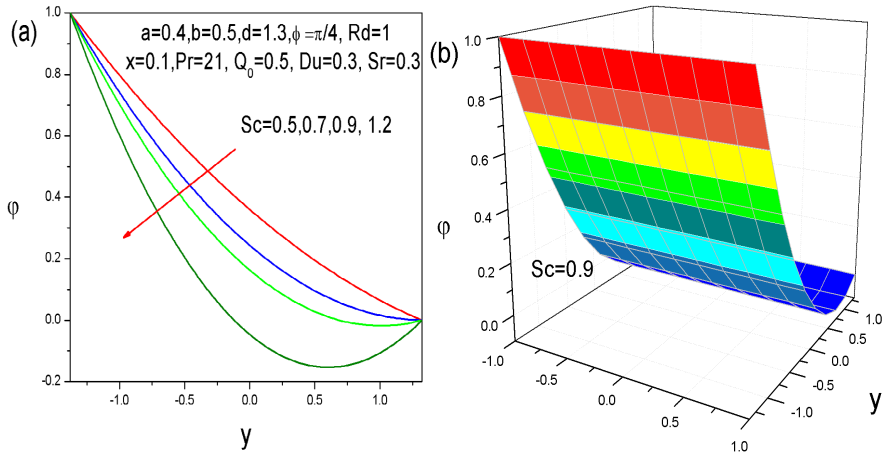

Figure 8. Concentration profiles for different *Sc* (a) 2D and (b) 3D.

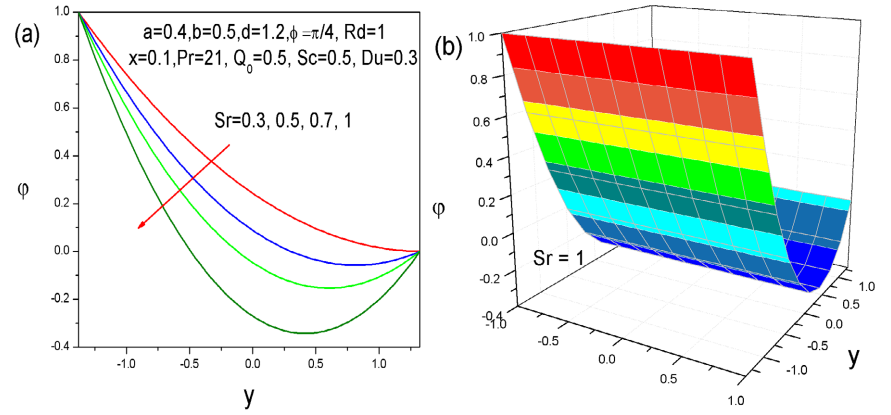

Figure 9. Concentration profiles for different *S*4 (a) 2D and (b) 3D.

The current study is contrasted with the earlier study [15] in order to confirm the accuracy of the numerical results. By taking equal parameters into consideration, both types of research have been brought to the same stage for comparison's sake (Newtonian instance). These comparisons, which are shown in **Figure 10**, show a very high degree of agreement.

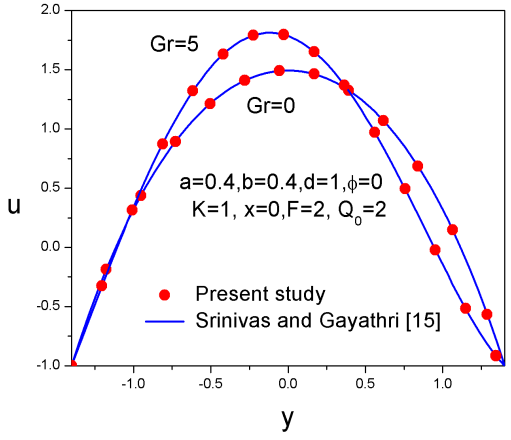

Figure 10. Comparison of velocity profiles (Newtonian Case).

6. Trapping Action

Peristaltic flow trapping is an additional noteworthy phenomenon. It depends on the process used to create streamlined shapes. Instead of traveling in the same direction as the peristaltic walls, the streamlines typically split and contain a fluid bolus in closed streamlines, which leads to the formation of a circulation zone. The motion of these trapped boluses and how they move with the wave in the flow illustrate the peristaltic flow trapping phenomena. To observe the impacts of M, K, β, and ϕ in the symmetric and asymmetric channels, I have sketched Figures 11-14.

Figure 11 displays streamlined graphs under the influence of a magnetic field. It is found that the size of the confined bolus decreases as M grows. M is the magnetic field parameter, which is the magnetic force divided by the inertia force. A rise in M intensifies the magnetic field, hence intensifying the Lorentz force, which is the body force. This force prevents the fluid from flowing freely.

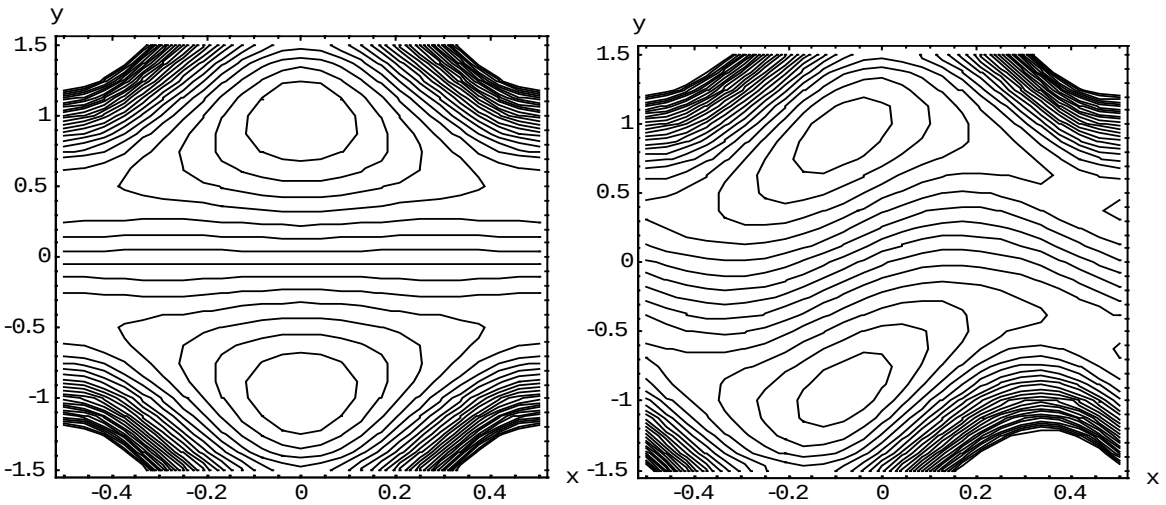

(a) $M=0, \phi=0$ (b) $M=0, \phi=\pi/3$

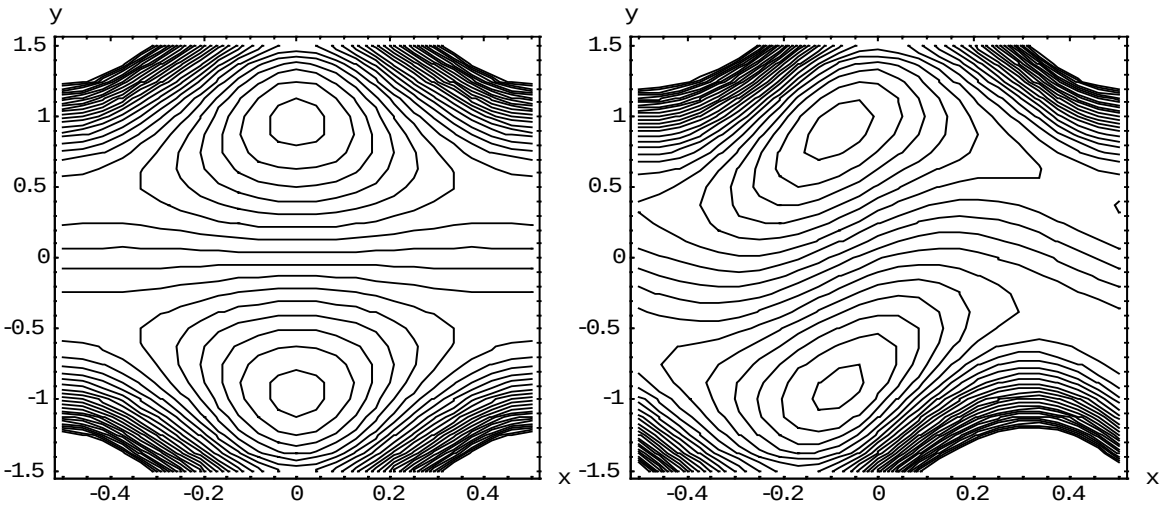

(c) $M=2, \phi=0$ (d) $M=2, \phi=\pi/3$

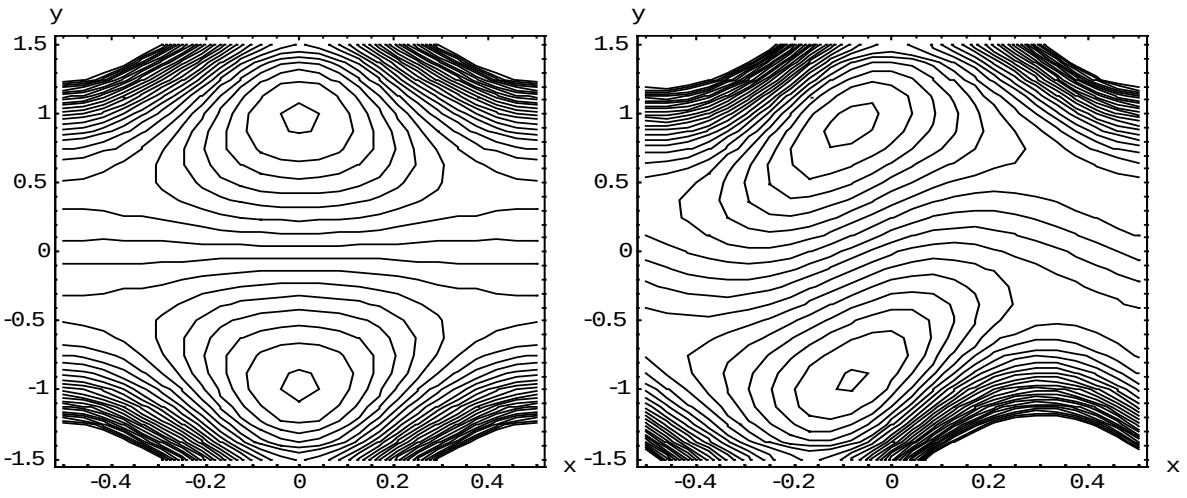

(e) $M=3,\phi=0$ (f) $M=3,\phi=\pi/3$

Figure 11. Streamlines for $a=0.5,b=0.5,d=1,q=-0.5,K=1,\beta=1$.

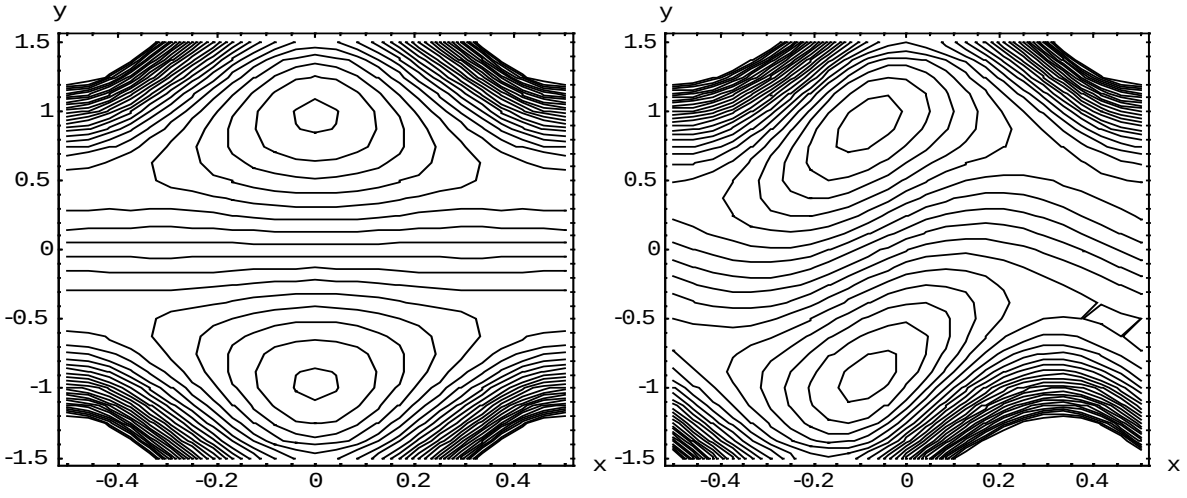

(a) $K=1,\phi=0$ (b) $K=1,\phi=\pi/3$

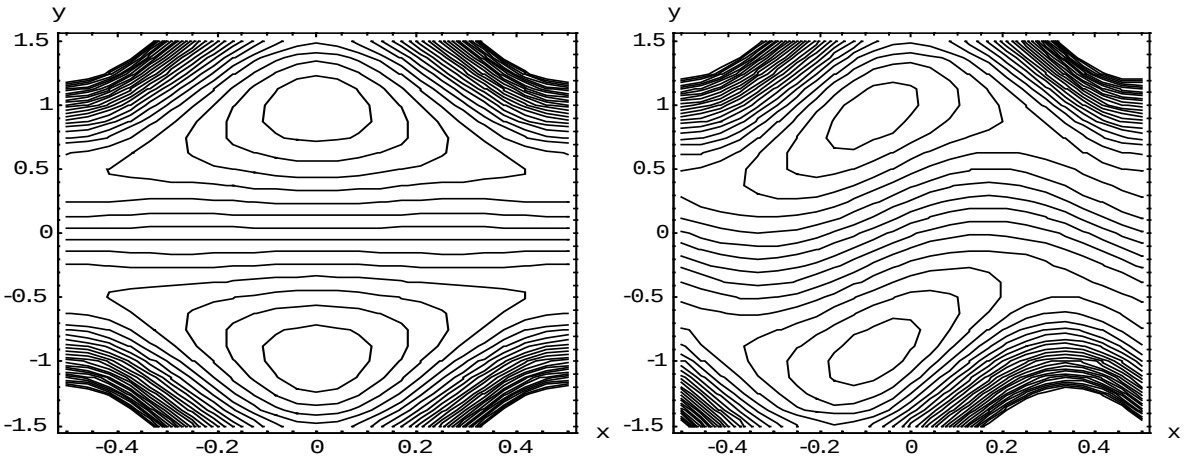

(c) $K=2,\phi=0$ (d) $K=2,\phi=\pi/3$

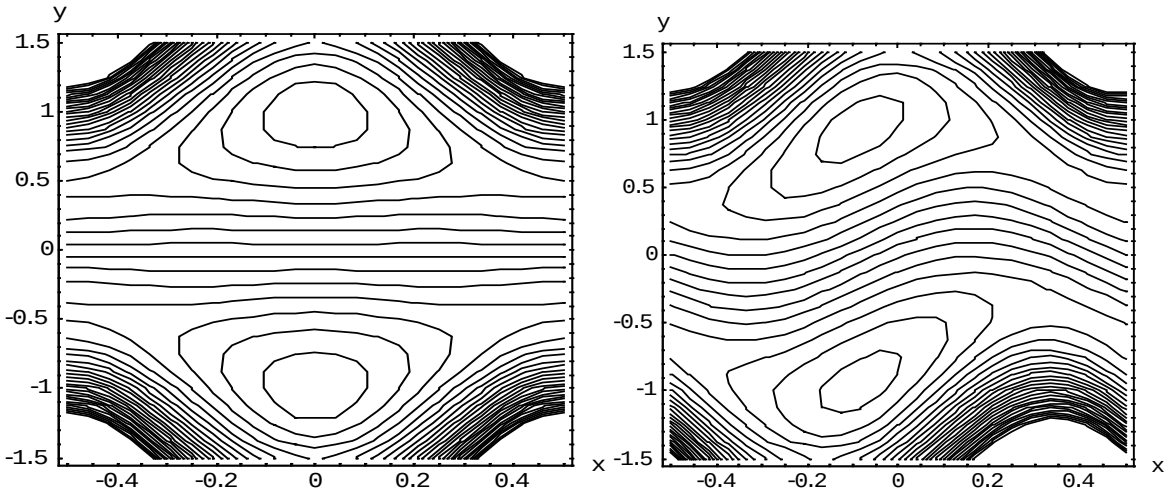

(e) $K=3,\phi=0$ (f) $K=3,\phi=\pi/3$

Figure 12. Streamlines for $a=0.5,b=0.5,d=1,q=-0.5,\beta=1,M=1$.

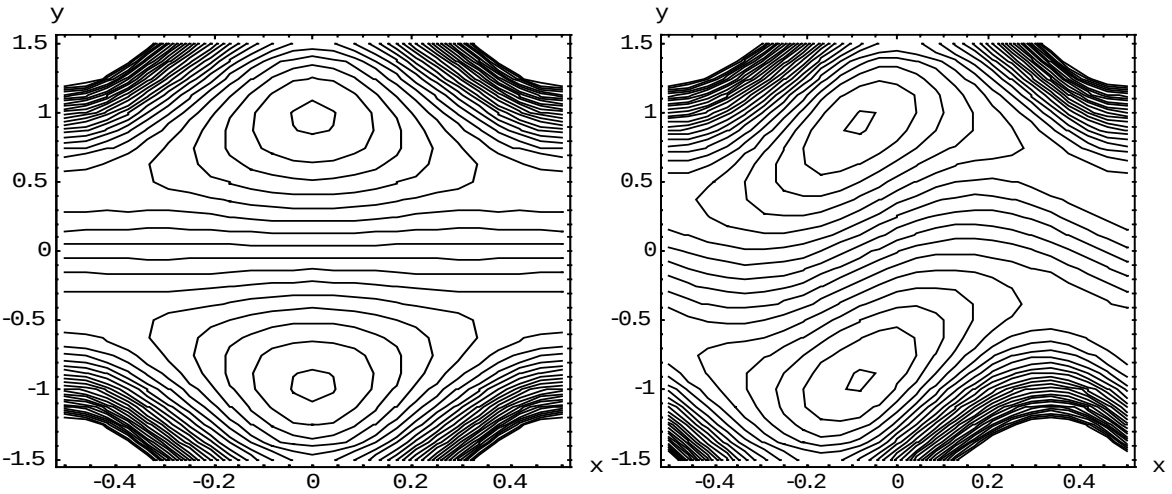

(a) $\beta=0.5,\phi=0$ (b) $\beta=0.5,\phi=\pi/3$

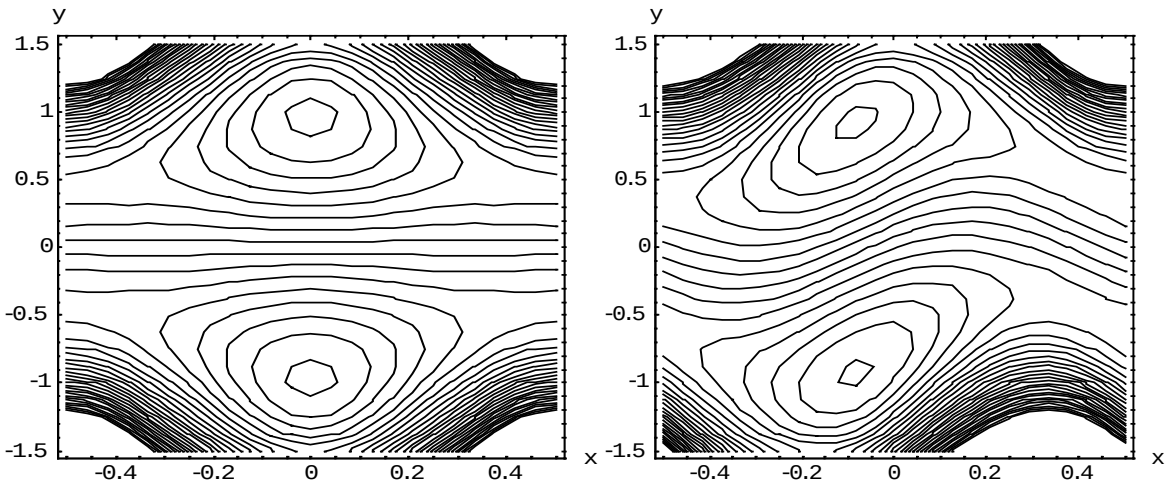

(c) $\beta=1,\phi=0$ (d) $\beta=1,\phi=\pi/3$

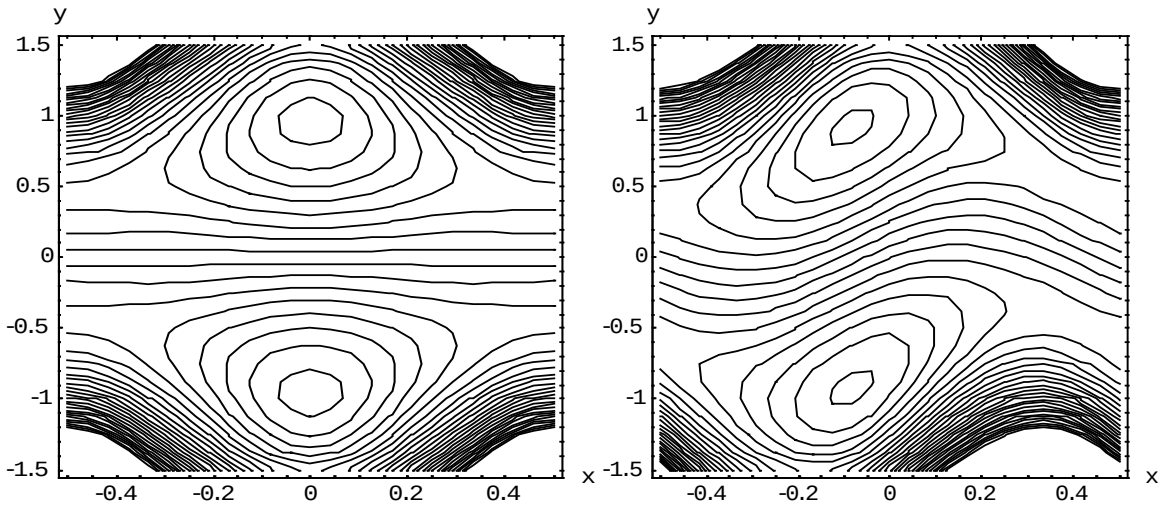

(e) $\beta = 3, \phi = 0$ (f) $\beta = 3, \phi = \pi/3$

Figure 13. Streamlines for $a = 0.5, b = 0.5, d = 1, q = -0.5, K = 1, M = 1$.

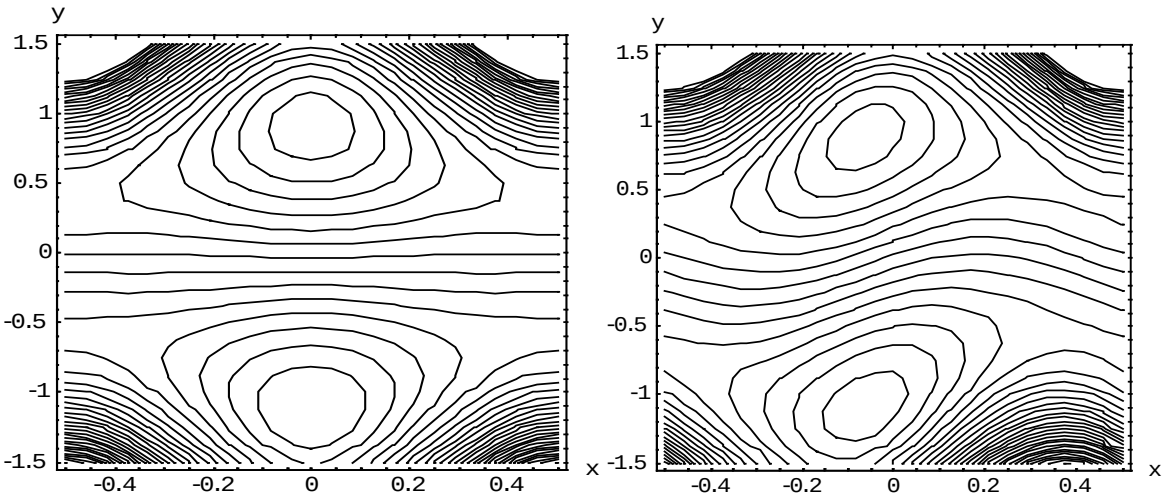

(a) $\phi = 0$ (b) $\phi = \pi/4$

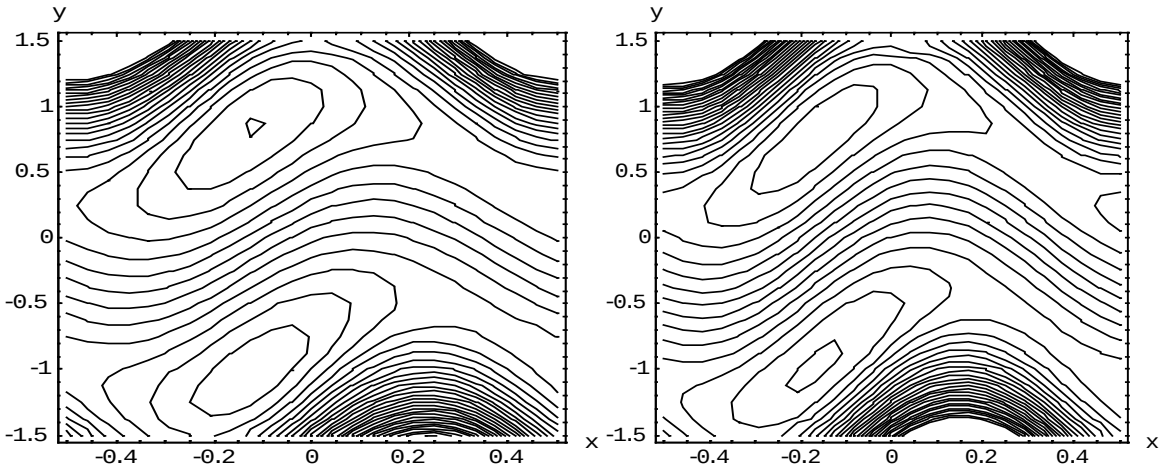

(c) $\phi = \pi/2$ (d) $\phi = 2\pi/3$

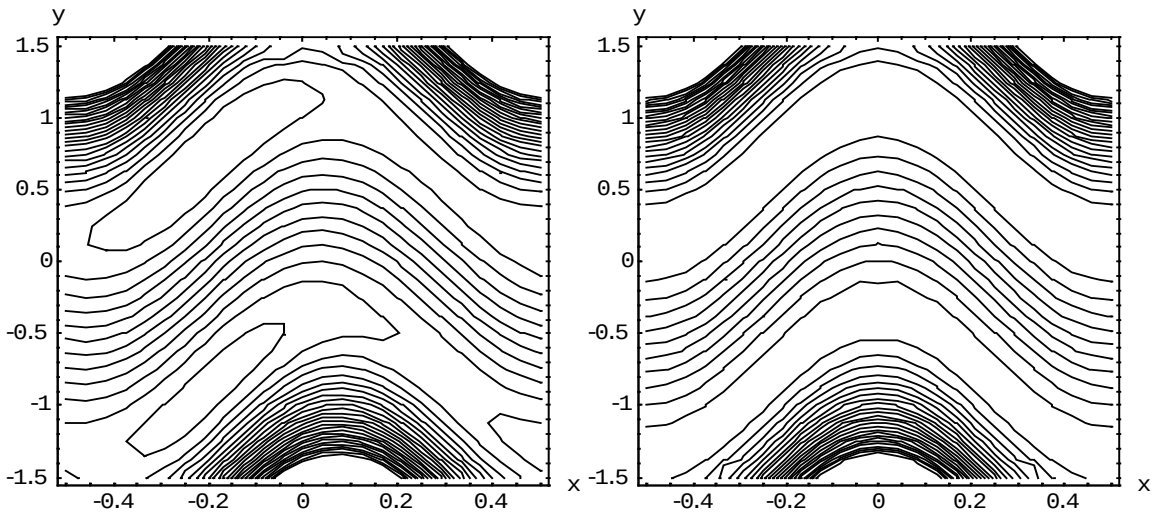

Figure 14. Streamlines for $a = 0.5, b = 0.5, d = 1, q = -0.5, K = 1, \beta = 1, M = 1$.

The effect of the permeability parameter K on streamlines is explored in Figure 12. The size of the trapped bolus increases as K increases. The permeability parameter K is not determined by the fluid itself, but rather by the properties of the porous media and the pore geometries. The flow velocity increases when K rises because the drag force decreases. This discovery offers empirical evidence in favor of the theory that peristaltic flow through a porous media causes fluid stiffness.

Figure 13 is outlined to show how streamlines vary for different values of the Casson fluid parameter β. The fluid becomes less viscous and thick when the Casson fluid parameter is increased, acting more like a Newtonian fluid. Consequently, the size of the trapping bolus expands with the Casson fluid parameter.

For different amounts of phase difference, the trapping pattern for symmetric $(a = b, d = 1, \phi = 0)$ and asymmetric channels is displayed in Figure 14. Observe that the size of the trapped bolus decreases with increasing ϕ, and disappears with increasing ϕ. Besides, the bolus moves upstream and decreases in size as ϕ increases.

7. Conclusions

In the presence of a magnetic field, this study examined heat and mass transfer in non-Newtonian peristaltic flow in a vertical channel. Numerical and analytical solutions are found. A graphic representation of how various parameters affect flow characteristics is shown. The study's primary conclusions are

1) Velocity field increases for K, β, Rd but decreases for M. This discovery has implications for the treatment of hypertension. When a patient undergoes an MRI while in a strong static magnetic field, the magnetic field idea can be profitably used to the imaging process.

2) Heat profiles rise in response to an increase in Du. However, the reverse

property for *Rd* is noted.

3) Soret number *Sr* plays a responsibility on concentration.

Conflicts of Interest

The authors declare no conflicts of interest regarding the publication of this paper.

References

[1] Bayliss, W.M. and Starling, E.H. (1899) The Movements and Innervation of the Small Intestine. *The Journal of Physiology*, **24**, 99-143. https://doi.org/10.1113/jphysiol.1899.sp000752

[2] Fetecau, C., Awan, A.U. and Fetecau, C. (2009) Taylor-Couette Flow of an Oldroyd-B Fluid in a Circular Cylinder Subject to a Time-Dependent Rotation. *Bulletin Mathématique de la Société des Sciences Mathématiques de Roumanie*, **52**, 117-128.

[3] Siddiqui, A.M., Hameed, M., Siddiqui, B.M. and Ghori, Q.K. (2010) Use of Adomian Decomposition Method in the Study of Parallel Plate Flow of a Third Grade Fluid. *Communications in Nonlinear Science and Numerical Simulation*, **15**, 2388-2399. https://doi.org/10.1016/j.cnsns.2009.05.073

[4] Khan, M., Maqbool, K. and Hayat, T. (2006) Influence of Hall Current on the Flows of a Generalized Oldroyd-B Fluid in a Porous Space. *Acta Mechanica*, **184**, 1-13. https://doi.org/10.1007/s00707-006-0326-7

[5] Siddiqui, A.M., Hameed, M., Siddiqui, B.M. and Babcock, B.S. (2012) Adomian De-Composition Method Applied to Study Nonlinear Equations Arising in Non-Newtonian Flows. *Applied Mathematical Sciences*, **6**, 4889-4909.

[6] Naz, R., Mahomed, F.M. and Mason, D.P. (2008) Comparison of Different Approaches to Conservation Laws for Some Partial Differential Equations in Fluid Mechanics. *Applied Mathematics and Computation*, **205**, 212-230. https://doi.org/10.1016/j.amc.2008.06.042

[7] Khalique, C.M. and Mahomed, F.M. (2009) Soil Water Redistribution and Extraction Flow Models: Conservation Laws. *Nonlinear Analysis*: *Real World Applications*, **10**, 2021-2025. https://doi.org/10.1016/j.nonrwa.2008.03.008

[8] Mekheimer, K.S., Husseny, S.Z. and Abd El Lateef, A.I. (2011) Effect of Lateral Walls on Peristaltic Flow through an Asymmetric Rectangular Duct. *Applied Bionics and Biomechanics*, **8**, 295-308. https://doi.org/10.1155/2011/424183

[9] Akram, S., Mekheimer, K.S. and Nadeem, S. (2014) Influence of Lateral Walls on Peristaltic Flow of a Couple Stress Fluid in a Non-Uniform Rectangular Duct. *Applied Mathematics & Information Sciences*, **8**, 1127-1133. https://doi.org/10.12785/amis/080323

[10] Yin, F. and Fung, Y.C. (1969) Peristaltic Waves in Circular Cylindrical Tubes. *Journal of Applied Mechanics*, **36**, 579-587. https://doi.org/10.1115/1.3564720

[11] Casson, N. (1959) Rheology of Disperse Systems. Pergamon Press, 84.

[12] Blair, S.G.W. and Spanner, D.C. (1974) Introduction to Biorheology by GW Scott Blair, Chapter XII on Botanical Aspects by DC Spanner.

[13] Neeraja, A., Renuka Devi, R.L.V., Devika, B., Naga Radhika, V. and Krishna Murthy, M. (2019) Effects of Viscous Dissipation and Convective Boundary Conditions on Magnetohydrodynamics Flow of Casson Liquid over a Deformable Porous

Channel. *Results in Engineering*, **4**, Article ID: 100040.
https://doi.org/10.1016/j.rineng.2019.100040

[14] Eldabe, N.T., Saddeck, G. and El-Sayed, A.F. (2001) Heat Transfer of MHD Non-Newtonian Casson Fluid Flow between Two Rotating Cylinders. *Mechanics and Mechanical Engineering*, **5**, 237-251.

[15] Srinivas, S. and Gayathri, R. (2009) Peristaltic Transport of a Newtonian Fluid in a Vertical Asymmetric Channel with Heat Transfer and Porous Medium. *Applied Mathematics and Computation*, **215**, 185-196.
https://doi.org/10.1016/j.amc.2009.04.067

Appendix

$$\alpha = \sqrt{\frac{M^2}{1+1/\beta} + \frac{1}{K}}$$

$$A = Q_0/(1 + Rd - PrDuScSr)$$

$$A_1 = (h_1 + h_2)A/2 + 1/(h_2 - h_1)$$

$$A_2 = h_1^2 A/2 - A_1 h_1$$

$$B_1 = -(h_1 + h_2)ScSrA/2 + 1/(h_2 - h_1)$$

$$B_2 = -ScSrh_1^2 A/2 - B_1 h_1$$

$$C_5 = \frac{\beta}{2\alpha^2(1+\beta)}(GrA_1 + GcB_1)$$

$$C_6 = \frac{\beta}{6\alpha^2(1+\beta)}(-GrA + GcAScSr)$$

$$P_1 = \alpha e^{\alpha h_1}/\left(e^{\alpha h_1} - e^{\alpha h_2}\right)$$

$$P_2 = e^{-\alpha h_1} - e^{-\alpha h_2}$$

$$P_3 = h_1^2 + h_1 h_2 + h_2^2 - 3(h_1 + h_2)/\alpha$$

$$P_4 = h_1 + h_2 - 2/\alpha$$

$$P_5 = \alpha e^{-\alpha h_1}$$

$$P_6 = -1 - F/(h_1 - h_2)$$

$$P_7 = -P_5 + P_1 P_2 - 2P_2/(h_1 - h_2)$$

$$P_8 = 2h_1 - P_4 - 2(h_1 - h_2)/\alpha$$

$$P_9 = 3h_1^2 - P_3 - 3P_1\left(h_1^2 - h_2^2\right)/\alpha$$

$$P_{10} = P_6 - C_5 P_8 - C_5 P_9$$

$$P_{11} = e^{\alpha h_1} - e^{\alpha h_2}$$

$$P_{12} = 2C_5(h_1 - h_2)/\alpha$$

$$P_{13} = 3C_6\left(h_1^2 - h_2^2\right)/\alpha$$

$$P_{14} = F/2 - C_5 h_1^2 - C_6 h_1^3$$

$$C_4 = P_{10}/P_7$$

$$C_3 = (C_4 P_2 - P_{12} - P_{13})/P_{11}$$

$$C_2 = -C_5 P_4 - C_6 P_3 + (F - 2C_4 P_2)/(h_1 - h_2)$$

$$C_1 = P_{14} - C_2 h_1 - C_3 e^{\alpha h_1} - C_4 e^{-\alpha h_1}$$